Analysis of Momentum Density Shifts in Carbon-Like Ions Using Kullback-Leibler Divergence

Riam Amer Ahmed and Wissam Ahmed Ameen
Department of Physics, University of Anbar, 650001 Anbar, Iraq
{rei20s2001, wissam.ameen }@uoanbar.edu.iq

Keywords: Roothaan-Hartree-Fock (RHF), Momentum Density Shift, KL-Divergence, Momentum Space.

Abstract: Roothaan-Hartree-Fock method was utilized to examine momentum density shifts in each of the shells of the carbon atom. The analysis is further expanded to include some carbon-like ions: N^{+1}, O^{+2} and F^{+3} in the ground state. The shift in the momentum density of adjacent ions within the isoelectronic series was analysed using the Kullback–Leibler divergence as an information-theoretic tool. They were found to have four distinct zones (two favouring the preceding ion in the isoelectronic sequence (lower nuclear charge) at low and high momenta and two favouring the succeeding ion in the isoelectronic sequence (higher nuclear charge) at intermediate and relatively high momenta). It was observed that the values of the Kullback-Leibler divergence of the identified momentum zones decrease in a systematic way with the nuclear charge, indicating an increasing similarity of the momentum-density distributions of the compared distributions. The shared momentum domain (core zone) is an overlapping grey zone, which typically escalated with ionisation. This alteration in the size of zoning is compatible with the principle of conservation of probability, when the density decreases in one zone and increases in another. The expectation values of various momentum moments were computed to optimize the interpretation of the momentum density shifts that were found using KL divergence.

1 INTRODUCTION

The radial momentum density function of one electron has been used in many studies to understand structural and dynamical characteristics of atom and ions. A number of efforts has been taken to sub-divide the distribution into specific areas. To illustrate this, Koga and Matsuyama (2005) divided the radial density functions into inner and outer parts of the 102 atoms in their ground state, He through *Lr*, and they found that the separation of the radial density functions brought out structural information that was not visible in the overall distribution. To give an example, the peaks of inner and outer shells can be distinguished distinctly, and each of the components can be attributed to various physical characteristics [1]. It has also been established that the methods of partitioning of momentum space can be generalized to molecular systems. In particular, Balanarayan and Gadre. (2006) adopted a Hirshfeld like partitioning of electron momentum density to obtain atom contributions to molecules and hence attributing p-space properties to chemical terms of charges, kinetic energies, directionality of bonds etc. [2]. Koga et.al (2007) also improved on their previous subdivision of the average electron radius into split direct and exchange terms in the framework of the Hartree-Fock theory. Their systematical examination of 102 atoms revealed that the electron exchange has a slight diminution impact on the inner radius and augmentation on the outer radius, which is, in effect, an expansion of the radial separation, albeit in an insignificant measure relative to the powerful direct influence [3]. Koga and Matsuyama (2010) expanded their inner-outer breakup of the radial density to singly-excited $1snl$ states of He. They showed that the inner density is comparable with the He^+ cation density with the outer density describing the excited electron, and that indices of radial separation and similarity are fine descriptors of states [4]. Rafid and Ameen (2025) report the existence of a zone-like structure within the radial density distribution of He isoelectronic series, in position space, of single atoms. They traced the evolution of zones due to boosting the nuclear charge. Their analysis is based on the conservation of charge density [5]. Nevertheless, this method was limited to one shell and was entirely based on a geometrical comparison. The Kullback-Leibler divergence is used to give an information theoretic value of the disparity

between two probability distributions [6]. It is among the comparison measures of probability distributions that is widely applied [7]. It has also been used in atomic systems to measure differences between density functions most notoriously, the Fisher and Jensen Sharon divergences have been used on atomic position and momentum space density distributions, Antolín, Angulo, and López-Rosa, (2009). Their findings revealed that these can be used to give quantitative data of shell structures and Fisher divergence can identify local characteristics and JSD global trends [8]. The authors of the article by Antolín, Angulo, Mulas, and López-Rosa. (2014) focused on information-theoretic divergence to study relativistic phenomena of the hydrogenic systems. Using Jensen Schrodinger and Dirac densities on position space and momentum space, the researchers used Jensen-Shannon measures and Jensen-Fisher measures to discover global and local properties of the electron distributions in complements [9]. In their article, Chatzisavvas *et al.* (2018) used the Kullback-Leibler divergence to compare the outcome of electron density distributions of the Roothaan-Hartree-Fock and the reference densities of a past study. In this respect, the KL measure indicated a strong and quantitative indicative measure of the change in the alternate characterization of the atomic densities, therefore, demonstrating that it could be able to identify fine architectural disparities [10]. The Kullback-Leibler divergence was also applied in other areas by Liu (2019), which confirmed that the Kullback-Leibler divergence is applicable in density functional reactivity theory, where the Kullback-Leibler divergence is justified to support electronic density partitioning programs, and also to compute reactivity descriptors in the sequence between He and *Kr* transition. It was already established in the paper that KL divergence does not merely allow to identify the deviations in densities, but also to obtain chemically useful information about the reallocation of electrons [11]. López-Rosa *et al.* (2021) extended the use of information-theoretic divergences to analyse pair density distributions in many-electron systems. Their study, carried out in both position and momentum spaces, demonstrated that such measures effectively capture electron correlation and reveal shell-filling patterns across the periodic table [12]. More recently, Hu et al. (2025) extended it to the nuclear physics scale by running KL divergence on Parton distribution functions, showing that KL divergence can be applied throughout the atomic to the subnuclear scale [13]. Although the remarkable development has been made in the past research, there is still the visible gap. Certain studies have tried to decompose position space density functional of individual shells and Kullback-Leibler divergence has been used to compare density distributions or to study correlations of electrons. But it is not yet directly made use of as a quantitative instrument to measure zone effects in momentum density, especially in the treatment of single shells. This is the major contribution of the current work. In this work, momentum density fluctuations have been determined, which occupy the momentum density into separate areas. An information-theoretic approach provides the analysis of the nature of these zones. The information-theoretic tool that is used is the Kullback-Leibler (KL) divergence. The experiment is concerned with carbon atom in its ground state. Then, it is extrapolated to the words of a few carbon-like ions N^{+1}, O^{+2} and F^{+3}in the ground state. The procedure that had to be followed to carry out the analytical calculations was Roothaan-HartreeFock approximation. The computational part had been calculated as a code with the assistance of Wolfram Language[14] to perform the computational part. The atomic data of Clementi and Roetti was employed [15].The atomic units are used throughout this work.

2 WAVEFUNCTION AND CALCUATIONS

The one-electron radial momentum density distribution is defined as the probability density of finding an electron with momentum between p and $p + dp$ from the nucleus [16]. It is obtained by integrating the reduced density function over all angular and spin coordinates in momentum space. This function provides complete information about all atomic properties that depend solely on electron momentum, such as the expectation value of the kinetic energy. Moreover, the position and shapes of the peaks in this function reflects the momentum localisation and shell structure of electronic systems [17]. To perform the momentum space analysis, using the Rootthaan-Hartree-Fock method, the reduced density function is defined as follows [18]:

$$\prod^{(2)}(y_1, \dots, y_2 | y_1', \dots, y_2') = \binom{N}{2} \int dy_{2+1} \dots dy_N \frac{\Phi^*(y_1', \dots, y_2', y_{2+1}, \dots, y_N)}{\Phi(y_1, \dots, y_N)} \quad (1)$$

Here, $\binom{N}{2}$ is the multiplicative binomial factor [19]. The wavefunction $\Phi(y_1, y_2, \dots, y_N)$ refers to the momentum representation of its counterpart, Ψ, in the

position space. It is obtained by applying the following Dirac-Fourier transformation [20], [21]:

$$\Phi(y_1, y_2, \dots, y_N) = (2\pi)^{-3N/2} \int \Psi\, e^{[-i\sum_{k=1}^{N} p_k \cdot r_k]} dr_1\, dr_2 \dots dr_N. \quad (2)$$

The wavefunction $\Phi(y_1, y_2, \dots, y_N)$ is defined in terms of momentum-spin coordinates $y_k = (p_k, \sigma_k\ )$, where the term p_k is the linear momentum of the K^{th} electron.

In this work, the concept of momentum density shifts, for a given shell, refers to the partial probability which is transferred from the i^{th} atom (or ion) to occupy a space within the partial probability of the $i+1$ atom due to boosting the atomic number by one unit:$|Z_i - Z_{i+1}| = 1$. The analysis of momentum density shifts across isoelectronic ions was conducted using the information-theoretic measure known as the Kullback–Leibler (KL) divergence. This approach allowed for a more nuanced and probabilistic characterisation of the shifts between adjacent momentum distributions in the isoelectronic series. The KL divergence was evaluated locally within each shift region $n = 1,2,3,4$, corresponding to distinct zones.

Given the inherent asymmetry of the Kullback–Leibler (KL) divergence(i.e.,$D_{KL}\big(I(p)_{z_i} \parallel I(p)_{z_{i+1}}\big) \neq D_{KL}\big(I(p)_{z_{i+1}} \parallel I(p)_{z_i}\big)$, its application in this study was guided by the direction of the momentum density shift between each pair of isoelectronic series. For every identified shift region, the KL divergence was computed based on which distribution dominates that region, as follows: In the first zone, depicted in yellow and third zone, depicted in blue regions, the shift favoured the atom or ion with lower nuclear charge (i.e., $I(p_1)_i$). Accordingly, the KL divergence was evaluated as [7], [22]:

$$D_{KL}^{(n)}\big[I(p)_{z_i} \parallel I(p)_{z_{i+1}}\big] = \int_{a_k}^{b_k} I(p)_{z_i} \ln\left(\frac{I(p)_{z_i}}{I(p)_{z_{i+1}}}\right) dp. \quad (3)$$

Both $I(p_1)_{z_i}$ and $I(p_1)_{z_{i+1}}$ represent the one-electron momentum density distribution for an atom (or ion) at momentum i and $i+1$ in the series, respectively:

$$I(p) = \int \Pi_{HF}^{(2)}(y_1, y_2)\, p_1^2\, p_2^2\, dp_2\, d\Omega_1 d\Omega_2\, d\sigma_1 d\sigma_2 \quad (4)$$

Here $d\Omega_k$ represents the angular part of the volume element, whereas $d\sigma_k$ indicates the spin element. In the second zone, depicted in green and fourth zone, depicted in orange, the shift was in favour of the ion with higher nuclear charge (i.e., $I(p)_{z_{i+1}}$). Thus, the direction was reversed:

$$D_{KL}^{(n)}\big[I(p)_{z_{i+1}} \parallel I(p)_{z_i}\big] = \int_{a_k}^{b_k} I(p)_{z_{i+1}} \ln\left(\frac{I(p)_{z_{i+1}}}{I(p)_{z_i}}\right) dp. \quad (5)$$

Here $n = 1,2,3,4$ refers to the four momentum density shift regions, while $[a_k, b_k]$ defines the momentum interval of the n^{th} region.

The overlapping zone (core zone), depicted in gray, was quantified using the overlap coefficient (OVL), defined as the integral of the minimum between the two probability density functions ($\Delta_{i,i+1}$) [23]:

$$\Delta_{i,i+1} = \int_0^\infty \min\big[I(\boldsymbol{p})_{z_i}\, ,\, ,\, ,\ I(\boldsymbol{p})_{z_{i+1}}\big] d\boldsymbol{p}. \quad (6)$$

This measure captures the shared probability mass between the two distributions. The one-electron expectation value is defined [24], [25]:

$$\langle p_1^n \rangle = \int_0^\infty I(\boldsymbol{p})\, p^n\, dp. \quad (7)$$

Where $-2 \leq n \leq 2$, in particular, most of the $\langle p_1^n \rangle$ moments have physical properties. For instance, $\langle p_1^2 \rangle$ is propertional to the nonrelativistic kinetic energy, while $\langle p_1^{-1} \rangle$ is simply the peak value of the Compton profile $J(q=0)$. $\langle p_1^0 \rangle$ must be equal one (normalization condition) [26].$\langle p_1^1 \rangle$ is propertional to the Slater- Dirac exchange energy [24].

3 RESULTS AND DISCUSSION

The one-electron pairs of adjacent atoms (or ions) momentum density distribution distribution and its expectation values in C isoelectronic series at ground state are examined to investigate the momentum density shift with the aid of Roothaan-Hartree-Fock wavefunction. One can note a consistent trend when the momentum distributions of the $1s_\alpha 1s_\beta$, $2s_\alpha 2s_\beta, 2px_\alpha 2py_\alpha$ intra-shells are discussed of both the carbon atom and its isoelectric series: N^{+1}, O^{+2} and F^{+3}. Physically, the growing nuclear charge causes the electronic orbitals to become contracted in the sense of position space, which suggests the momentum distributions to become spread around to higher momentum values as illustrated in Figures 1-6. This is represented by a rightward movement of the distribution's peaks along the momentum axis, and by a slowing down of the intensity of the peaks with the increased momentum dispersion, and the diminished probability of finding electrons at low momentum values. The two relations below can be used to summaries the trend: $p_1^C < p_1^{N^{+1}} < p_1^{O^{+2}} < p_1^{F^{+3}}$ and $|I(p_1)_{max}|^C > |I(p_1)_{max}|^{N^{+1}} > |I(p_1)_{max}|^{O^{+2}} > |I(p_1)_{max}|^{F^{+3}}$.

Here, p_1 is the location at which the peak occurs as indicated in Figure 1.

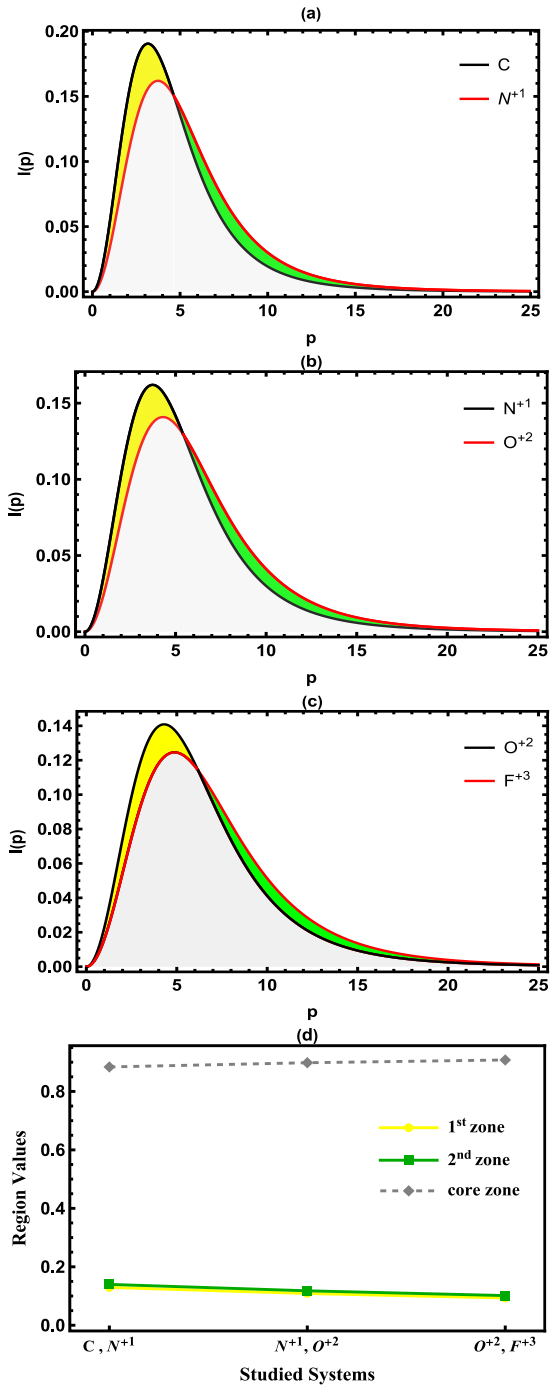

Figure 1: One-particle momentum density distribution $I(p_1)_{1s_\alpha 1s_\beta}$ for $1s_\alpha 1s_\beta$ shell. The first three plots represent pairs of C-like ions starting from $(a)C,,,N^{+1}$ $(b)N^{+1},,,O^{+2}$ $(c)O^{+2},,,F^{+3}$(d) presents the values of the KL-Divergence-based shift zones D_{KL}^{n} and the core zone $\Delta_{i,i+1}$ across the studied sequence.

The KullbackLeibler (KL) divergence was here in used as an information-theoretic measure to measure the density change between every two successive pairs $(C,,,,N^{+1})$, $(N^{+1},,,O^{+2})$, $(O^{+2},,,F^{+3})$. The separation was calculated in different momentum regions. The distribution of the less-charged and more-charged ion respectively was made the reference distribution in the respective regions in which the shift was being directed (i.e. the region dominated with the momentum in its favour), and the reverse when the shift was being directed toward the higher-charged ion. The distributions were found to consist of four main areas which were different regions: This work also has the yellow zone also known as the first zone.

It represents a change to the less-charged ion, and it is usually in the low-momentum domain, and is more densely distributed. The KL value at this region is the measure of the loss of the low momentum representation when there is an increase in the nuclear charge. The second zone represents the zone which is said to be a green zone. It is a transformation to the more charged ion and the transformation is typically at the intermediate to high momentum range. According to it, it exists that there is increased overlap of the orbitals because the nuclear attraction is stronger. Light blue zone is represented as the third zone. It is clearly observed at the $2s_\alpha 2s_\beta$ beta shell. It is an outer orbit which is present in the tail of the momentum distribution, indicating a leftover by the less-charged ion in the extreme high momentum values. This region decays slowly with the increasing nuclear charge as the nodal radial structure peculiar to the $2s_\alpha 2s_\beta$Lastly, the central zone that is represented by the grey color is shown as an overlap zone. It is calculated as the horizontal sum of the point wise minimum of the two distributions. It represents the extent to which they are similar, and its value to the extent to which they are charged, showing a general convergence of the electronic momentum distribution as the ions are more tightly bound together.

According to Figure 1a, b, c, the KL divergence values in both subspaces of the $1^{st} and 2^{nd}$ zones, are all low (<0.14 a.u.). In stark contrast, the core zone had all very high values (>0.88 a.u.) for all pairs of ions irrespective of electron momentum (Fig. 1d). This indicates that, for all ions in the $1s_\alpha 1s_\beta$ shell, the corresponding momentum distributions were the same, which indicates a massive overlap in momentum distributions. This was most likely the case because this energy shell is closest to the nucleus, and, as a result, electrons would have essentially the same rather strong attraction from the

nucleus leading to very little overall variation in momentum space.

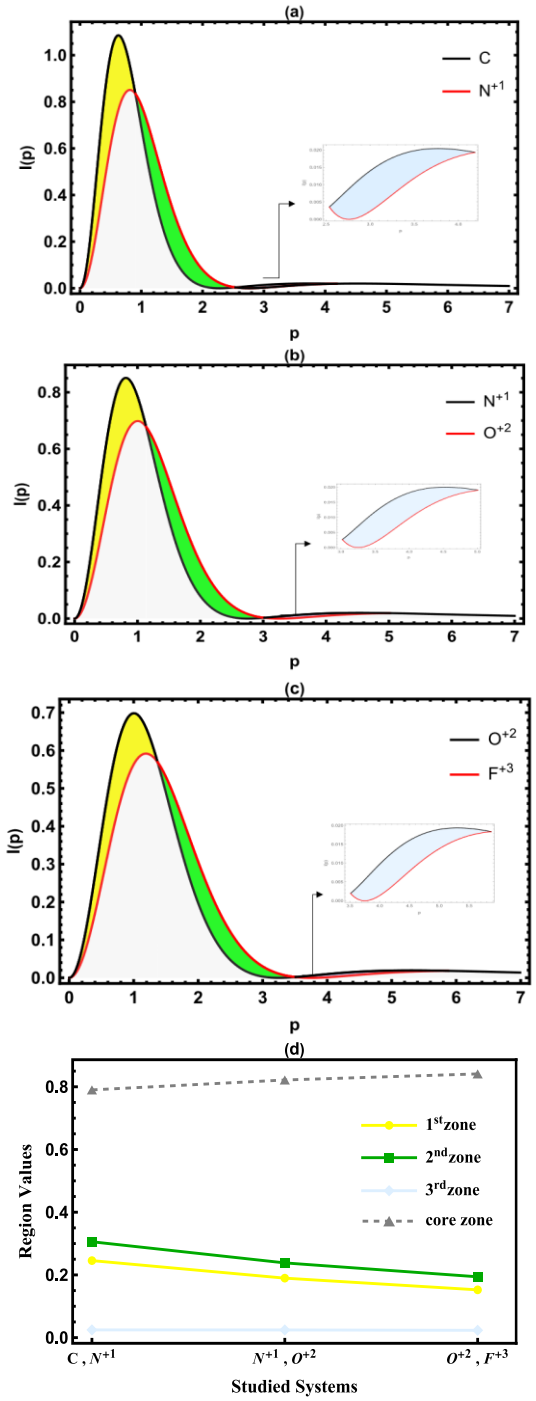

Figure 2: One-particle momentum density distribution $I(p_1)_{2s_\alpha 2s_\beta}$ for $2s_\alpha 2s_\beta$ shell. The first three plots represent pairs of C-like ions starting from $(a)\ C,,,N^{+1}\ (b)N^{+1},,,O^{+2}\ (c)O^{+2},,,F^{+3}$. (d) presents the values of the KL-Divergence-based shift zones D_{KL}^{n} and the core zone $\Delta_{i,i+1}$ across the studied sequence.

Figure 2a-d reveals that $2s_\alpha 2s_\beta$ shell, both yellow and green zones (up to ~0.25 and up to (~0.30),) have a significant value of KL divergence, respectively. Also, a light blue region is formed, indicating that there is a longer momentum tail in the favour of the less-charged ion, indicating that there are more high-momentum components. Moreover, the values of the KL divergence in all locations of the momentum shift are steadily decreasing with an increased nuclear charge. The values of the core regions are expected to decrease relative to the $1s_\alpha 1s_\beta$ This implies that the transformative changes of the $2s_\alpha 2s_\beta$ momentum distribution are much more significant than others, probably because it contains a radial node. The $2s_\alpha 2s_\beta$ shells are more sensitive to the variation of the nuclear charge, leading to an increase in the momentum differences of the nearest ions.

The 1^{st} was observed to have the largest KL divergence between all three shells in the configurations of the subshell $2px_\alpha 2py_\alpha$ illustrated in Figure 3a-d with a maximum of 0.33 in certain configurations. The values of divergence also became much large in the second zone with values up to the (~0.25–0.35)$a.u.$.The central area is the lowest (in terms of values) (~0.740.84) a.u., which indicates the minimal similarity between the corresponding distributions. This is an example of weakest overlap in distributions of core zone 2p shells. It is also the subshell ($2px_\alpha 2py_\alpha$) in which the nuclear charge is significantly sensitive due to the anisotropic shape and the behavior of the orbitals being rather complex.

Nevertheless, although it shows the greatest KL divergence of all the shells considered, the values in the shell themselves steadily decrease with increase of nuclear charge (i.e., from (C, N^{+1}), (N^{+1}, O^{+2}), (O^{+2}, F^{+3}), a gradual decrease in momentum shift with ionisation.

A specific trend was found in the momentum distribution curves of the successive inter-shell ion pairs, 1s_α 2p_xα ,2s_α 2p_xα and 1s_α 2s_α as shown in Figures 4-6. It was found that the values of KL divergence between the shift regions (i.e., 1^st, 2^nd, 3^rd, and 4^th) tended to fall with the increase in the nuclear charge, indicating an increasing agreement between the electronic momentum distributions of the respective pair. Conversely, the size of the core zone where the two distributions coincided with each other in all instances showed a conspicuous growth, which is an indication of increasing informational similarity with the growth of nuclear charge.

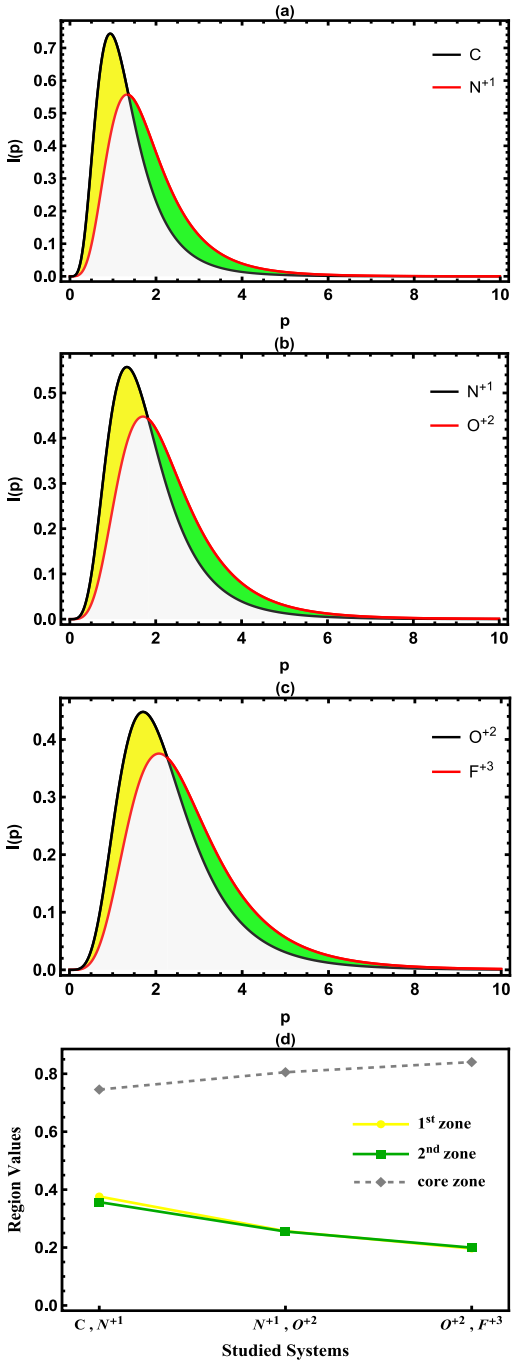

Figure 3: One-particle momentum density distribution $I(p_1)_{2p_{x\alpha}2p_{y\alpha}}$ for $2p_{x\alpha}2p_{y\alpha}$ shell. The first three plots represent pairs of C-like ions starting from $(a)\ C,,,N^{+1}\ (b)N^{+1},,,O^{+2}\ (c)O^{+2},,,F^{+3}$. (d) presents the values of the KL-Divergence-based shift zones D_{KL}^{n} and the core zone $\Delta_{i,i+1}$ across the studied sequence.

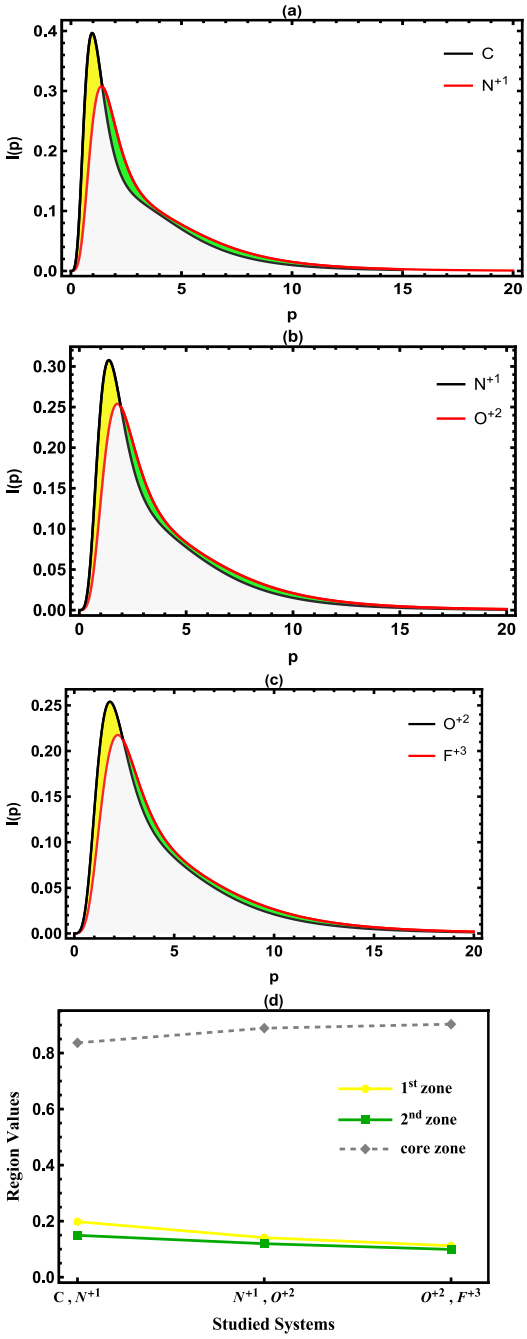

Figure 4: One-particle momentum density distribution $I(p_1)_{1s_\alpha 2p_{x\alpha}}$ for $1s_\alpha 2p_{x\alpha}$ shell. The first three plots represent pairs of C-like ions starting from $(a)\ C,,,N^{+1}\ (b)N^{+1},O^{+2}\ (c)O^{+2},F^{+3}$. (d) presents the values of the KL-Divergence-based shift zones D_{KL}^{n} and the core zone $\Delta_{i,i+1}$ across the studied sequence.

Figure 4 a, c depicting I(p_1) of 〖1s〗 _α 2p_xα shell. Figure 4a comparing C and N^(+1), indicates the biggest yellow contribution, which suggests a strong shift towards the neutral carbon at low momentum. The 2^ndzone on the other hand is humble and only indicates a partial compensation of N^(+1) at intermediate momentum. Figure 4b which compares N^(+1) with O^(+2)shows that there is a visible decrease in both 1^st and 2^nd zone indicating that the two ion are becoming structurally closer. Lastly, the comparison of O^(+2)with F^(+3) in 4c shows the smallest 1^stand 2^nd one in the entire series, and the grey core zone is as the most noticeable. The quantitative validation of these observations is explained in Figure 4d: the 1^st area is becoming smaller as per the sequence, and the 2^nd one is smaller and decreases quicker all the time. Meanwhile the grey core zone increases a bit, proving the point of view that the similarity of the world is increased with the increase of nuclear charge. This has been demonstrated to be consistent with the uncertainty principle: the more localised the position space (i.e. large Z) the more spread, but increasingly uniform, are the momentum distributions.

Conversely, the $2s_\alpha 2p_{x\alpha}$ Inter-shell, as depicted in Figure 5 (a, b, c, d) only had two shift regions (1^{st} and 2^{nd}). In this case, the zone of core grew gradually with nuclear charge meaning that the distributions converged more. In the 1^{st} zone, the change in the KL values was found to decrease between 0.25127 in pair C, N^{+1} to 0.1905, and further to 0.1550 in pair O^{+2}, F^{+3}. On the same note, in the 2nd zone, the divergence went down to 0.2646 to 0.2102, and then lower to 0.1729. Conversely, the values of the core zone rose significantly with the increase in nuclear charge, going through 0.80003 in C, N^{+1} to 0.8299 in N^{+1}, O^{+2}, and then to 0.8490 in O^{+2}, F^{+3}.. This action indicates a growing level of resemblance between the distributions in line with radial contraction effects that are caused by a stronger nuclear attraction.

This growing overlap is explained by the fact that the two orbitals lie in the same energy level ($n=2$) which means radial proximity and energetic compatibility such that the orbitals can exhibit more momentum space interference, especially as they contract with each other as a result of the growing nuclear charge.

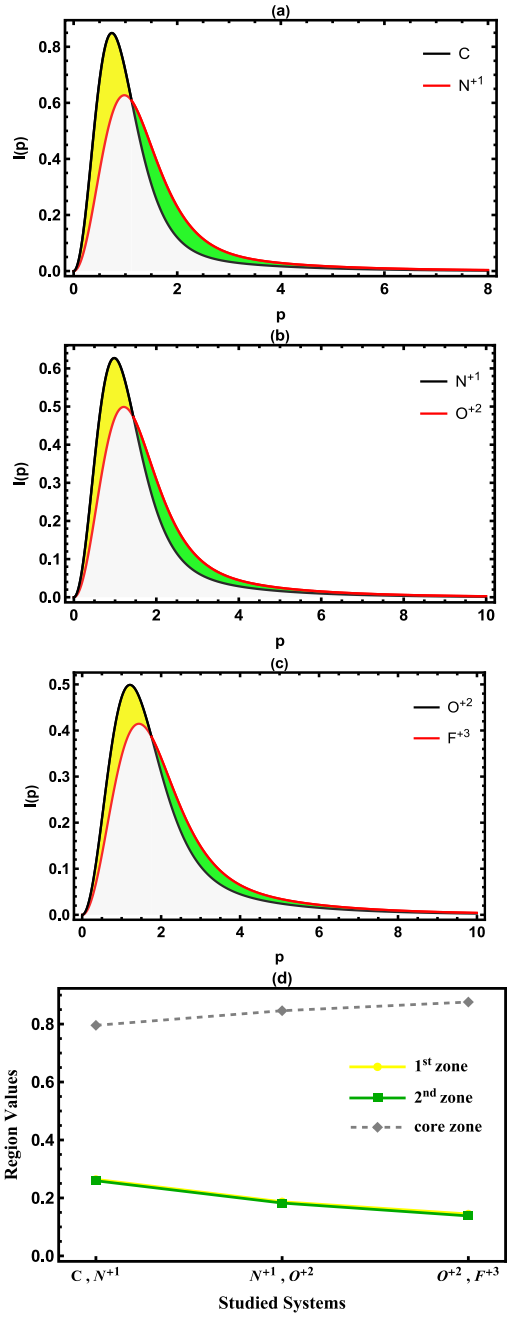

Figure 5: One-particle momentum density distribution $I(p_1)_{2s_\alpha 2p_{x\alpha}}$ for $2s_\alpha 2p_{x\alpha}$ shell. the first three plots represent pairs of C-like ions starting from $(a)\ C,, N^{+1}$ $(b) N^{+1},, O^{+2}$ $(c) O^{+2}, F^{+3}$. (d) presents the values of the KL-Divergence-based shift zones D_{KL}^n and the core zone $\Delta_{i,i+1}$ across the studied sequence.

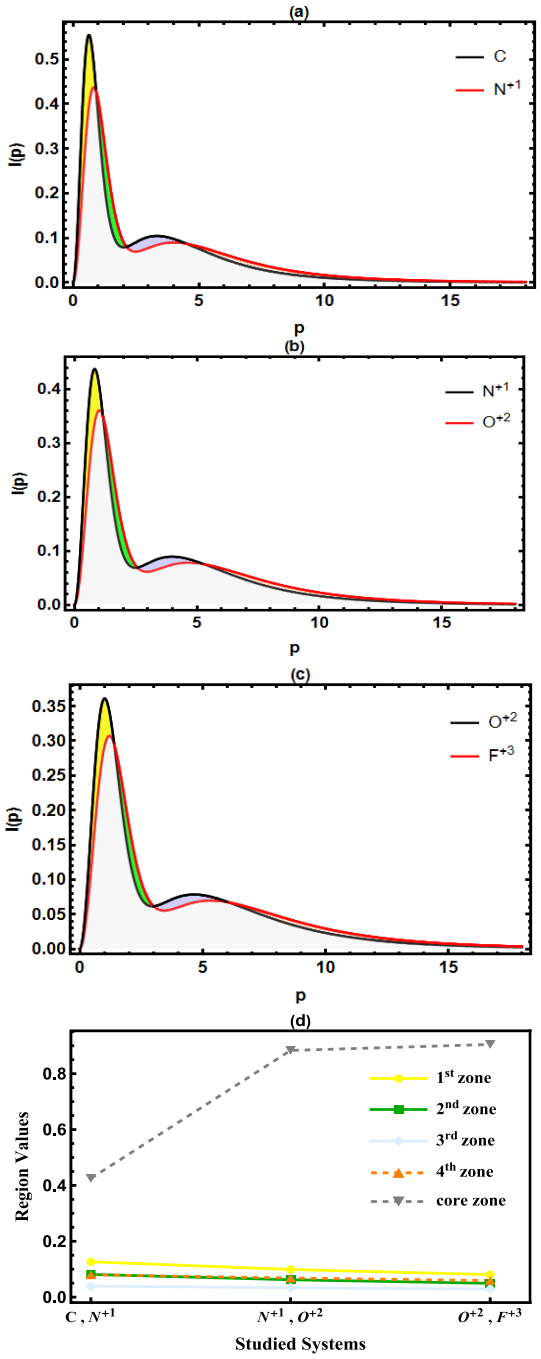

Figure 6: One-particle momentum density distribution $I(p_1)_{1s_\alpha 2s_\alpha}$ for $1s_\alpha 2s_\alpha$ shell. The first three plots represent pairs of C-like ions starting from $(a)\ C,,N^{+1}$ $(b)N^{+1},O^{+2}$ $(c)O^{+2},,F^{+3}$. (d) presents the values of the KL-Divergence-based shift zones D_{KL}^{n} and the core zone $\Delta_{i,i+1}$ across the studied sequence.

The inter-shell $1s_\alpha 2s_\alpha$ inter-shell as indicated in Figure $(6-a,,,b,,,c,,,d)$, was the most complicated with four different zones of shifts (1^{st}, 2^{nd}, 3^{rd}, and 4^{th}). The analysis showed that there was an impressive non-linear rise in core zone values which increased significantly between 0.4249 $(C,,,N^{+1})$, to 0.8831 $(N^{+1},,,O^{+2})$, and reached a maximum of 0.9046 $(O^{+2},,,F^{+3})$. The cause of this large increase is that radial similarity between two orbitals of the same general type (e.g. both s-type) allows a larger overlap in momentum space. Moreover, the radial node of the higher orbital adds to a longer range of overlap of momentum.

This orbital interaction is exaggerated as the two orbital contract due to the increased nuclear interaction. The KL divergence values in the four regions of the shift, show that the nuclear charge decreases C to N^{+1} and O^{+2} then to F^{+3}. In 1^{st}zone (the low-momentum yellow zone), the divergence values decrease from 0.1265 $(C,,,,,N^{+1})$ to 0.0989 $(N^{+1},,,,,O^{+2})$, and further to 0.0867 (O^{+2},F^{+3}), respectively, and there is an increasing similarity between the momentum distributions of the inner and the outer orbitals. The same downward trend is noted with 2^{nd} zone with values of 0.0814 to 0.0622 and then to 0.0495 respectively of the same ion pairs. Particularly, the 3^{rd}zone and 4^{th} zone respectively, that are both high-momentum tail regions of the distributions, are also observed to have a consistent decrease in KL divergence: the values of the blue region decrease to 0.0397 to 0.03340 and then to 0.0289, whereas the values of the orange region decrease 0.0799 to 0.0604 and finally to 0.0599. All these trends are indicative of increased momentum space overlap and structural compatibility between 1s and 2s orbitals with increasing nuclear potential.

The Table 1 shows the expectation values $\langle p^n \rangle$ of some of the values of power $(n = -2,,,-1,,,0,,,1,,2)$ of individual electron shells (i.e. intra and inter-shell) in the carbon atom and its isoelectric ions (N^{+1}, O^{+2}, F^{+3}) at the ground state by using (7). The value of $\langle p^0 \rangle$ is equal to one, reflecting the normalisation condition of the momentum density function. The $\langle p^{-1} \rangle$ moment, which is associated with the peak of the Compton profile at $q = 0$, decreases systematically with increasing nuclear charge.

Table 1: The one-particle expectation values $\langle p_1^n \rangle$ where $-2 \leq n \leq 2$, for individual shell within C-like ions in (a.u.).

Shell	C-like ions	$\langle p_1^{-2} \rangle$	$\langle p_1^{-1} \rangle$	$\langle p_1^{0} \rangle$	$\langle p_1^{1} \rangle$	$\langle p_1^{2} \rangle$
$1s_\alpha 1s_\beta$	C	0.165240	0.306422	1	4.76983	32.1035
	N^{+1}	0.118808	0.260149	1	5.6105	44.3315
	O^{+2}	0.089546	0.225942	1	6.4528	58.5506
	F^{+3}	0.069816	0.199609	1	7.2957	74.766
$2s_\alpha 2s_\beta$	C	4.47919	1.61125	1	1.0863	3.07712
	N^{+1}	2.65756	1.24291	1	1.4152	5.04622
	O^{+2}	1.75606	1.0103	1	1.7502	7.53924
	F^{+3}	1.2475	0.851064	1	2.0879	10.5446
$2p_{x\alpha} 2p_{y\alpha}$	C	1.23452	0.959633	1	1.3747	2.50736
	N^{+1}	0.625794	0.690089	1	1.8672	4.50987
	O^{+2}	0.385048	0.543825	1	2.3435	7.00906
	F^{+3}	0.262138	0.450046	1	2.8123	10.0092
$1s_\alpha 2s_\alpha$	C	2.32223	0.958842	1	2.9283	17.5902
	N^{+1}	1.3882	0.751534	1	3.5127	24.6887
	O^{+2}	0.922784	0.61811	1	4.1013	33.0456
	F^{+3}	0.658663	0.525339	1	4.6911	42.655
$1s_\alpha 2p_{x\alpha}$	C	0.69988	0.633029	1	3.0720	17.3054
	N^{+1}	0.372303	0.475121	1	3.7388	24.4205
	O^{+2}	0.237299	0.384883	1	4.39789	32.7798
	F^{+3}	0.165977	0.324828	1	5.05395	42.3876
$2s_\alpha 2p_{x\alpha}$	C	2.85686	1.28544	1	1.2306	2.79224
	N^{+1}	1.64168	0.966499	1	1.64137	4.77807
	O^{+2}	1.07054	0.777056	1	2.0468	7.27414
	F^{+3}	0.754823	0.650557	1	2.4498	10.2769

This indicates a decline in central momentum density due to the contraction of the spatial distribution. This trend is especially evident in the $1s_\alpha 1s_\beta$ shell, where the value drops from 0.306 $a.u.$ in carbon to 0.199 $a.u.$ in F^{+3}. Simultaneously, $\langle p^2 \rangle$, which relates to the nonrelativistic kinetic energy, increases substantially, from 32.1$a.u.$ in C to 74.7 $a.u.$ for F^{+3} in the same shell, highlighting the intensification of Coulombic confinement and the contraction of the radial extent of the wavefunction. Similar trends are observed in the outer shells such as $2s_\alpha 2s_\beta$ and$2p_{x\alpha} 2p_{y\alpha}$, albeit with smaller numerical values. The $\langle p^{-2} \rangle$ moment, which reflects the spatial delocalisation of the wavefunction in real space, gradually decreases with increasing Z, indicating a shift of the momentum distribution towards higher momentum values. In contrast, $\langle p^1 \rangle$ and $\langle p^2 \rangle$ increase with ionisation, corresponding to a rise in kinetic energy and a compression of real-space spread. For inter-shell configurations such as $1s_\alpha 2s_\alpha$, $1s_\alpha 2p_{x\alpha}$, and $2s_\alpha 2p_{x\alpha}$, the expectation values follow similar trends. For example, in the $1s_\alpha 2p_{x\alpha}$ state, $\langle p^{-2} \rangle$ decreases from (0.699 to 0.165)$a.u$, while $\langle p^2 \rangle$ rises from (17.3 to 42.4)$a.u$, reflecting the increasing contribution of high-momentum components due to overlap between orbitals from different shells. These inter-shell states show comparatively higher $\langle p^{-2} \rangle$ values at low Z than the outer shells, indicating a broader spatial extent resulting from weaker Coulombic attraction.

Overall, all $\langle p^n \rangle$ moments exhibit a consistent pattern that reflects the nature of momentum-space contraction under increasing nuclear charge: moments associated with low momentum $\langle p^{-2} \rangle$, $\langle p^{-1} \rangle$ decrease, while those linked to energy and high momentum ($\langle p^1 \rangle$, $\langle p^2 \rangle$) increase. This behaviour signals a progressive shift of the momentum distribution towards higher momentum regions due to the enhanced Coulombic confinement. The results for $1s_\alpha 1s_\beta$, $2s_\alpha 2s_\beta$, $2px_\alpha 2py_\alpha$ $shells$ in carbon agree well with the results of comparing ref [27].

4 CONCLUSIONS

This study used a systematic study of the momentum density shifts in the C-like ions using the Kullback-Leibler divergence as a measure of information. The main result is a strictly decreasing tendency of KL

divergence values in subsequent pairs of ions, which is observed and is accompanied by a corresponding extension of the common area of distribution. This is a strong indication of convergence of electronic momentum distribution which is a direct result of the enhanced nuclear attraction that pulls electron clouds together. Subsequent analysis of the momentum distribution revealed that the momentum distribution peaks move to higher momentum values with increment in ionisation, at the same time, showing decreasing intensity in the peaks. The increase in value of $\langle p^1 \rangle, , , \langle p^2 \rangle$, and and decrease in value of $\langle p^{-2} \rangle, , , \langle p^{-1} \rangle$ values confirm the momentum shift toward higher ranges. These results provide evidence that the electrons become more strongly localised in p-space as Z increases. The new KL divergence option in the application has offered a fine-tuning of quantifying the momentum density shifts and has given deep understanding of the structural changes of an atomic system under ionisation. In addition to its theoretical significance, the proposed methodology establishes a solid foundation for extending information studies to more complex atomic systems. Future work may investigate electron correlation effects using post-Hartree-Fock methods, and extend the investigation to heavier iso-electronic series. Additionally, integrating Compton profile measurements would help bridge the gap between theoretical analysis and experimental validation. This form of methodology has a lot of potential in the future of electronic structure research.

REFERENCES

[1] T. Koga and H. Matsuyama, “Inner and outer radial density functions in many-electron atoms,” Theor Chem Acc, vol. 115, no. 1, pp. 59–64, Jan. 2006.

[2] P. Balanarayan and S. R. Gadre, “Atoms-in-molecules in momentum space: A Hirshfeld partitioning of electron momentum densities,” The Journal of Chemical Physics, vol. 124, no. 20, p. 204113, May 2006.

[3] T. Koga and H. Matsuyama, “Direct and exchange contributions to inner and outer radii in many-electron atoms,” Theor Chem Account, vol. 118, no. 5–6, pp. 931–935, Nov. 2007.

[4] H. Matsuyama and T. Koga, “Inner and outer radial density functions in singly-excited 1snl states of the He atom,” Journal of computational and applied mathematics, vol. 233, no. 6, pp. 1584–1589, 2010.

[5] R. A. Asal and W. A. Ameen, “Charge shift in He isoelectronic series using the Hartree-Fock method,” in AIP Conference Proceedings, AIP Publishing LLC, 2025, p. 020016.

[6] S. Kullback and R. A. Leibler, “On information and sufficiency,” The annals of mathematical statistics, vol. 22, no. 1, pp. 79–86, 1951.

[7] V. Bonnici, “A Maximum Value for the Kullback–Leibler Divergence between Quantized Distributions,” Information, vol. 15, no. 9, p. 547, Sep. 2024.

[8] J. Antolín, J. C. Angulo, and S. López-Rosa, “Fisher and Jensen–Shannon divergences: Quantitative comparisons among distributions. Application to position and momentum atomic densities,” The Journal of Chemical Physics, vol. 130, no. 7, p. 074110, Feb. 2009.

[9] J. Antolín, J. C. Angulo, S. Mulas, and S. López-Rosa, “Relativistic global and local divergences in hydrogenic systems: A study in position and momentum spaces,” Phys. Rev. A, vol. 90, no. 4, p. 042511, Oct. 2014.

[10] K. Ch. Chatzisavvas, Ch. C. Moustakidis, and C. P. Panos, “Information entropy, information distances, and complexity in atoms,” The Journal of Chemical Physics, vol. 123, no. 17, p. 174111, 2018.

[11] S. Liu, “Identity for Kullback-Leibler divergence in density functional reactivity theory,” The Journal of Chemical Physics, vol. 151, no. 14, Oct. 2019.

[12] S. López-Rosa, J. C. Angulo, A. L. Martín, and J. Antolín, “Analysis of correlation and ionization from pair distributions in many-electron systems,” Eur. Phys. J. Plus, vol. 136, no. 7, p. 763, Jul. 2021.

[13] S.-M. Hu, A.-S. Xiong, J. Xu, F.-S. Yu, and J.-X. Yu, “An analysis of nuclear parton distribution function based on Kullback-Leibler divergence,” 2025.

[14] W. R. Inc, “Mathematica, Version 12.1.” [Online].Available:https://www.wolfram.com/mathematica

[15] E. Clementi and C. Roetti, “Roothaan-Hartree-Fock atomic wavefunctions: Basis functions and their coefficients for ground and certain excited states of neutral and ionized atoms, Z≤ 54,” Atomic data and nuclear data tables, vol. 14, no. 3–4, pp. 177–478, 1974.

[16] A. Sarsa, F. J. Gálvez, and E. Buendía, “Correlated one-body momentum density for helium to neon atoms,” J. Phys. B: At. Mol. Opt. Phys., vol. 32, no. 9, pp. 2245–2255, May 1999.

[17] F. J. Gálvez, E. Buendía, and A. Sarsa, “One- and two-body densities of carbon isoelectronic series in their low-lying multiplet states from explicitly correlated wave functions,” The Journal of Chemical Physics, vol. 124, no. 4, p. 044319, Jan. 2006.

[18] P.-O. Löwdin, “Quantum Theory of Many-Particle Systems. I. Physical Interpretations by Means of Density Matrices, Natural Spin-Orbitals, and Convergence Problems in the Method of Configurational Interaction,” Phys. Rev., vol. 97, no. 6, pp. 1474–1489, Mar. 1955.

[19] A. J. Thakkar, “The Momentum Density Perspective of the Electronic Structure of Atoms and Molecules,” in Advances in Chemical Physics, 1st ed., vol. 128, S. A. Rice, Ed., Wiley, 2003, pp. 303–352.

[20] “Self-consistent field, with exchange, for beryllium,” Proc. R. Soc. Lond. A, vol. 150, no. 869, pp. 9–33, May 1935.

[21] P. Kaijser and V. H. Smith, “Evaluation of Momentum Distributions and Compton Profiles for Atomic and Molecular Systems,” in Advances in Quantum Chemistry, vol. 10, Elsevier, 1977, pp. 37–76.

[22] S. S. Wani et al., “Classifying deviation from standard quantum behavior using the Kullback-Leibler divergence,” EPL, vol. 144, no. 6, p. 62003, Dec. 2023.

[23] O. Al-Saidy, H. M. Samawi, and M. F. Al-Saleh, “Inference on overlap coefficients under the Weibull distribution: Equalshape parameter,” ESAIM: Probability and Statistics, vol. 9, pp. 206–219, 2005.

[24] W. M. Westgate, R. P. Sagar, A. Farazdel, V. H. Smith, A. M. Simas, and A. J. Thakkar, “Momentum-space properties of the neutral atoms from H through U,” Atomic Data and Nuclear Data Tables, vol. 48, no. 2, pp. 213–229, Jul. 1991.

[25] S. López-Rosa, J. C. Angulo, and J. S. Dehesa, “Spreading measures of information-extremizer distributions: applications to atomic electron densities in position and momentum spaces,” Eur. Phys. J. D, vol. 51, no. 3, pp. 321–329, Mar. 2009.

[26] A. Zarzo, J. C. Angulo, and J. Antolin, “A study of the atomic momentum density by means of radial expectation values,” J. Phys. B: At. Mol. Opt. Phys., vol. 26, no. 24, pp. 4663–4669, Dec. 1993.

[27] J. M. G. Delavega and B. Miguel, “Orbital and Total Atomic Momentum Expectation Values with Roothaan-Hartree-Fock Wave Functions,” Atomic Data and Nuclear Data Tables, vol. 54, no. 1, pp. 1–51, May 1993.